



# Understanding the nature of vanadium species supported on activated carbon and its catalytic properties in the aerobic oxidation of aromatic alcohols

Qinghu Tang, Yuanting Chen, Yanhui Yang\*

School of Chemical and Biomedical Engineering, Nanyang Technological University, Singapore 637459, Singapore

## ARTICLE INFO

### Article history:

Received 10 March 2009  
Received in revised form 19 August 2009  
Accepted 31 August 2009  
Available online 8 September 2009

### Keywords:

Vanadium oxide  
Activated carbon  
Alcohol oxidation  
Raman  
X-ray absorption  
XPS  
ESR

## ABSTRACT

Vanadium oxide catalysts supported on activated carbon (V/AC) with V loadings ranging from 1 to 20 wt.% were prepared by a wet-impregnation method. Various physicochemical characterization techniques, including nitrogen physisorption, X-ray diffraction (XRD), Raman spectroscopy, X-ray absorption (XANES and EXAFS), X-ray photoelectron spectroscopy (XPS), and electron spin resonance (ESR), were employed to understand the nature of vanadium species on activated carbon. The results revealed that vanadium oxide mainly existed in a highly dispersed state for 10 wt.% or less vanadium loadings; a large amount of vanadium resulted in aggregated microcrystalline phase. Vanadium species on activated carbon surface showed a similar local coordination structure to that of  $\text{NH}_4\text{VO}_3$  with a distorted tetrahedral symmetry at low vanadium loadings, whereas octahedral coordination was dominant at high vanadium loadings (>10 wt.%). All V/AC samples showed  $\text{V}^{5+}$  as the major oxidation state. Nevertheless,  $\text{V}^{4+}$  centered in a distorted tetrahedral symmetry could be detected at a vanadium loading greater than 4 wt.%. The catalytic activity for the benzyl alcohol oxidation largely depended on the dispersion, oxidation state, and local coordination of vanadium oxides on activated carbon. Highly dispersed vanadium ( $5+$ ) species with a distorted tetrahedral coordination were postulated to account for the excellent catalytic performances of V/AC catalysts ( $\text{TOF} = 39.1 \text{ h}^{-1}$ ).

© 2009 Elsevier B.V. All rights reserved.

## 1. Introduction

Supported vanadium oxide catalysts have been extensively engaged in various oxidation reactions, e.g., oxidation of alcohols to aldehydes or ketones, partial oxidation of hydrocarbons, oxidative dehydrogenation of alkanes to alkenes, oxidation of *o*-xylene to phthalic anhydride, sulfur dioxide oxidation, ammoxidation of aromatic hydrocarbons, and selective catalytic reduction (SCR) of nitrogen oxides [1–20]. Most studies revealed that the catalytic activity and selectivity of supported vanadium oxide catalysts mainly depended on the nature of vanadium active sites, e.g., oxidation state, dispersion of vanadium, local symmetry, and the metal-support interaction [21–23].

Activated carbon (AC) possesses quite a few unique characteristics that make this material very valuable as a catalyst support, such as high surface area, tunable porosity, high stability in caustic and acidic conditions, and rich surface chemistry due to the surface oxygen complexes [24]. Activated carbon-supported catalysts exhibit several advantages compared to silica- and alumina-supported catalysts. Interaction between support and active component is minimized to a large extent due to the inert graphitic surface, which

leads to an optimized utilization of active sites. Several studies have been reported on vanadium oxide supported on carbon materials [18–20,25–31]. However, some ambiguities about the insight of catalytically active vanadium sites still remain unsolved. It is unclear whether the vanadium oxides are present in the form of single oxidation state or a mixture of oxidic phases. The local coordination of vanadium has not been undoubtedly elucidated as well.

The present work is aimed to prepare a series of vanadium-containing catalysts supported on activated carbon (V/AC) by a conventional wet-impregnation method and to characterize the physicochemical properties of vanadium species using various techniques such as nitrogen physisorption, XRD, Raman, X-ray absorption, XPS, and ESR. The catalytic oxidation of aromatic alcohols is employed to evaluate the catalytic activity of as-prepared vanadium catalysts, with emphasis on understanding the nature of vanadium species formed on activated carbon in conjunction with finding the correlation between the surface vanadium species and the catalytic activity.

## 2. Experimental

### 2.1. Catalyst preparation

High purity activated carbon (Scharlau Chemie) was pretreated using  $\text{HNO}_3$  (1 M) before use. After washing with deionized water

\* Corresponding author. Tel.: +65 6316 8940; fax: +65 6794 7553.  
E-mail address: [yhyang@ntu.edu.sg](mailto:yhyang@ntu.edu.sg) (Y. Yang).

and drying, the BET surface area was  $856 \text{ m}^2 \text{ g}^{-1}$  with a total ash content below 0.1 wt.%. Ammonium metavanadate (99.8%) was chosen as the vanadium precursor. The V/AC catalysts were prepared by a wet-impregnation method. A required amount of ammonium metavanadate was dissolved in a 2 M oxalic acid solution and mixed with the AC support (vanadium loadings of 1–20 wt.%). The excess water was slowly evaporated in a water bath under continuous stirring. The residues were further dried in a vacuum oven at 393 K overnight and treated at 673 K for 3 h in a helium flow of  $30 \text{ ml min}^{-1}$ .

## 2.2. Characterization

Nitrogen physisorption was carried out at 77 K with a static volumetric Autosorb 6 (Quanta Chrome). Prior to the measurement, the samples were outgassed at 473 K to a residual pressure below  $10^{-4}$  Torr. A Baratron pressure transducer (0.001–10 Torr) was used for low-pressure measurements. The specific surface area was calculated by the standard BET method.

Powder X-ray diffraction (XRD) patterns were recorded using a Bruker Advance 8 X-ray diffractometer equipped with a rotating anode using  $\text{Cu K}\alpha$  radiation ( $\lambda = 0.154 \text{ nm}$ ), operating at 40 kV and 40 mA.

Raman spectra were collected on a Renishaw in Via Raman Microscope system with a 325 nm laser as the excitation source. A laser output of 30 mW was employed and the maximum incident power at the sample was approximately 6 mW.

The X-ray photoelectron spectroscopy (XPS) was measured on a VG Escalab 250 spectrometer equipped with an Al anode (Al  $\text{K}\alpha = 1846.6 \text{ eV}$ ). The background pressure in the analysis chamber was lower than  $1 \times 10^{-7}$  Pa. Measurements were performed using 20 eV pass energy, 0.1 eV step and 0.15 dwelling time. Energy correction was carried out using the C1s peak of adventitious C at 284.6 eV.

ESR spectra were measured using a Bruker EMX ESR spectrometer at the X-band ( $\sim 9 \text{ GHz}$ ). The powder sample was loaded into a quartz tube with inner diameter of 3 mm and measured at 77 K.

X-ray absorption measurements at vanadium K-edge were performed at the X-ray demonstration and development beam line of the Singapore Synchrotron Light Source (SSLS) where a Si (1 1 1) channel-cut monochromator was equipped [32]. The samples were ground, pressed into self-supporting wafers, placed in a stainless steel cell, and measured in transmission mode at room temperature. The electron energy in the storage ring was about 700 MeV with a current of about 200 mA. EXAFS spectra in transmission mode were recorded from 5350 to 6350 eV. Incident and transmitted X-ray intensities were measured by two ionization chambers filled with pure nitrogen. Energy was calibrated using V foil (5465.0 eV). The spectra collected were analyzed using WinXAS 2.3, an XAS data analysis program. The theoretical EXAFS functions for vanadium oxide species generated by the FEFF6 were used to fit the experimental data to calculate the V–O shell coordination numbers [33].

## 2.3. Catalytic reaction

The catalytic oxidation of aromatic alcohols with molecular  $\text{O}_2$  was carried out using a bath-type reactor operated under atmospheric condition. In a typical reaction run, a certain amount of catalyst was loaded to a 50 ml glass flask pre-charged with 2 mmol aromatic alcohol and 10 ml toluene, the mixture was then heated to the reaction temperature (373 K) under vigorous magnetic stirring (800 rpm). Oxygen flow was bubbled at a flow rate of  $10.0 \text{ ml min}^{-1}$  into the mixture to start the reaction once the reaction temperature was reached. Dodecane was used as the internal standard. After reaction, the solid catalyst was filtered off and the liquid organic

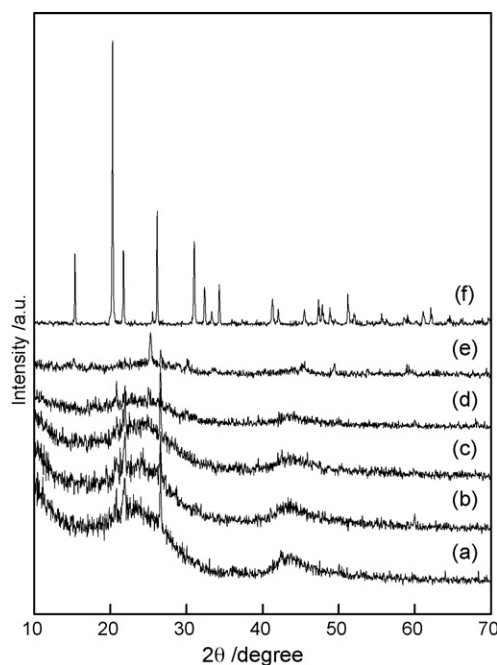


**Fig. 1.** X-ray diffraction patterns of the V/AC catalysts as well as  $\text{V}_2\text{O}_5$ : (a) activated carbon; (b) 1 wt.% V/AC; (c) 4 wt.% V/AC; (d) 10 wt.% V/AC; (e) 20 wt.% V/AC; (f)  $\text{V}_2\text{O}_5$ .

products were analyzed by an Agilent gas chromatograph 6890 equipped with a HP-5 capillary column (see Refs. [34,35] for detail information).

## 3. Results and discussion

### 3.1. XRD results

The powder X-ray diffraction patterns of V/AC catalysts with various vanadium loadings are shown in Fig. 1. Diffraction patterns of  $\text{V}_2\text{O}_5$  and activated carbon support are also included for compar-

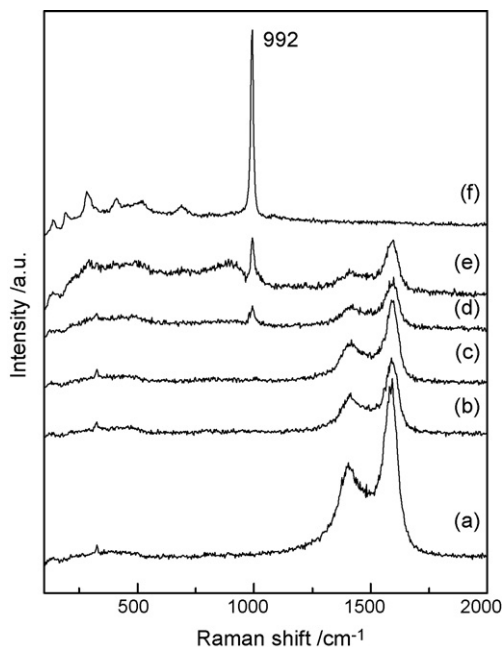


**Fig. 2.** Raman spectra of the V/AC catalysts as well as  $\text{V}_2\text{O}_5$ : (a) activated carbon; (b) 1 wt.% V/AC; (c) 4 wt.% V/AC; (d) 10 wt.% V/AC; (e) 20 wt.% V/AC; (f)  $\text{V}_2\text{O}_5$ .

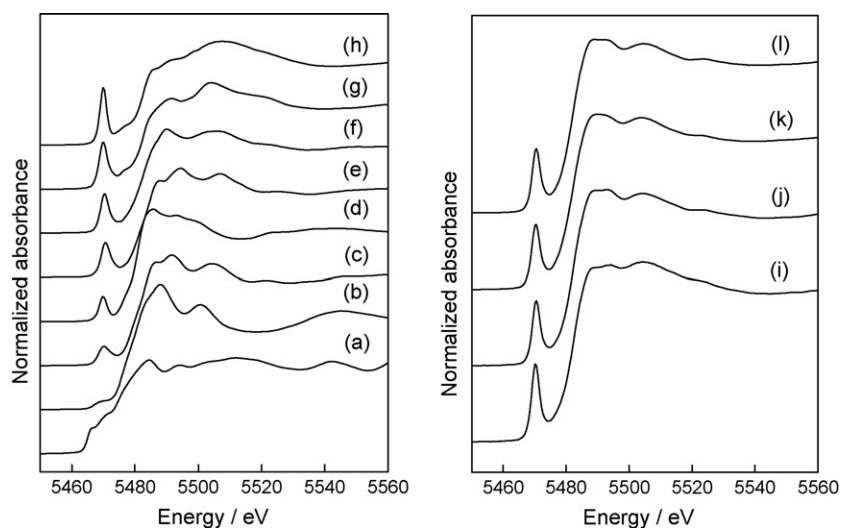


**Fig. 3.** V K-edge XANES spectra for the V/AC catalysts and the reference compounds: (a) V foil; (b)  $V_2O_5$ ; (c)  $VO_2$ ; (d)  $VOSO_4 \cdot 3H_2O$ ; (e)  $V_2O_5$ ; (f)  $PbV_2O_6$ ; (g)  $NH_4VO_3$ ; (h)  $Na_3VO_4$ ; (i) 1 wt.% V/AC; (j) 4 wt.% V/AC; (k) 10 wt.% V/AC; (l) 20 wt.% V/AC.

ison. Only broad diffraction patterns due to the activated carbon support can be observed when the V-content is lower than 10 wt.%. The absence of any crystalline vanadium oxide patterns indicates vanadium oxide species are highly dispersed on carbon surface. The V/AC samples with vanadium loadings greater than 10 wt.% show X-ray reflections at  $25^\circ$ ,  $30^\circ$ ,  $34^\circ$ ,  $45^\circ$ , and  $49^\circ$  (Fig. 1d and e), the intensity gradually increasing with the increase in the vanadium loading. The appearance of these XRD peaks is attributed to the formation of a crystalline vanadium oxide phase on carbon support. It is reported that a two-dimensional structure and  $V_2O_5$  crystallites become prevalent in high-loading  $VO_x/Al_2O_3$  and  $VO_x/SiO_2$  catalysts [7,36]. However, an interesting observation on these V/AC catalysts is that the crystalline phases of vanadium oxide presented in the V/AC samples are appreciably different from  $V_2O_5$  crystallites, evidenced by dissimilar X-ray diffraction patterns compared to that of  $V_2O_5$  (Fig. 1d and e vs. Fig. 1f).

### 3.2. Raman results

The Raman spectra of V/AC samples along with  $V_2O_5$  reference are shown in Fig. 2. The  $V_2O_5$  reference spectrum shows several distinct Raman peaks at 992, 689, 522, 409, 282, 198 and 141  $cm^{-1}$  (Fig. 2f), which are in good agreement with the literature reported elsewhere [37]. The Raman band located at 992  $cm^{-1}$ , which is primarily due to the symmetric stretch of V=O groups in the bulk vanadium oxides [38], can be clearly discerned for the V/AC sam-

ples with vanadium loadings higher than 10 wt.%. For V/AC samples with low vanadium loadings (<4 wt.%), no Raman feature assigned to crystalline vanadium oxides can be observed, and only Raman bands ascribed to activated carbon appear (Fig. 2b and c), implying that vanadium domains in these samples are highly dispersed on activated carbon surface. A typical Raman band at  $\sim 1040\text{ cm}^{-1}$  attributed to a characteristic of the V=O isolated species is observed on numerous oxide matrix supports with highly dispersed vanadium oxides [39,40]. However, the absence of this distinct feature in V/AC samples at low vanadium loadings may imply that the local coordination structure of vanadium species on activated carbon is unique.

### 3.3. X-ray absorption results

X-ray absorption spectroscopy is employed to further characterize the local symmetry of vanadium oxide structure supported on activated carbon. The normalized vanadium K-edge X-ray absorption near edge structure (XANES) spectra of V/AC samples along with reference vanadium compounds are shown in Fig. 3. All spectra exhibit a strong pre-edge absorption feature corresponding to the forbidden transition  $1s \rightarrow 3d$  [41], which is mainly caused by mixing the 4p orbital of vanadium and 2p orbital of the oxygen with the  $3d\pi$  orbital of vanadium atoms [41]. The XANES results for V/AC samples as well as reference vanadium compounds are summarized in Table 1. The pre-edge height and intensity are closely

**Table 1**  
Energy positions of various spectral features in the V K-edge XANES spectra.

Sample ID	Pre-edge position <sup>a</sup> (eV)	Main-edge position <sup>a,b</sup> (eV)	$E_{\text{pre-edge}} - E_0$ (eV)	$E_{\text{edge}} - E_{\text{pre-edge}}$ (eV)	Pre-edge peak height (a.u.)	Pre-edge peak intensity <sup>c</sup> (a.u.)
$Na_3VO_4$	5469.9	5482.4	4.9	12.5	0.65	1.77
$NH_4VO_3$	5470.1	5481.9	5.1	11.8	0.53	1.85
$PbV_2O_6$	5470.5	5482.1	5.5	11.6	0.45	1.55
$V_2O_5$	5470.8	5481.0	5.8	10.2	0.39	1.54
$VOSO_4 \cdot 3H_2O$	5469.7	5477.9	4.7	8.2	0.28	0.90
$V_2O_4$	5470.1	5478.5	5.1	8.4	0.22	–
$V_2O_3$	5469.7	5475.5	4.7	5.8	0.10	–
1 wt.% V/C	5470.1	5482.2	5.1	12.1	0.51	1.67
4 wt.% V/C	5470.4	5482.3	5.4	11.9	0.43	1.40
10 wt.% V/C	5470.4	5482.0	5.4	11.6	0.42	1.45
20 wt.% V/C	5470.5	5482.0	5.5	11.5	0.42	1.43

<sup>a</sup> The uncertainty in peak positions estimated to be  $\pm 0.2$  eV.

<sup>b</sup> Main-edge position is chosen as the mid point of the absorption jump.

<sup>c</sup> Peak intensity is calculated by peak height  $\times$  width at half maximum.

related to the local symmetry, and they can be used to gain insight into the coordination structure when one compares the compounds with a known model coordination environment [41]. The height of pre-edge peak monotonically decreases as the vanadium structure changes from the tetrahedral coordination ( $\text{Na}_3\text{VO}_4$ ) to the square pyramidal ( $\text{V}_2\text{O}_5$ ) or the octahedral coordination ( $\text{PbV}_2\text{O}_6$ ). As shown in Table 1, the 1 wt.% V/AC sample presents a lower pre-edge peak compared to the reference compound  $\text{Na}_3\text{VO}_4$  (tetrahedral) but similar to that of  $\text{NH}_4\text{VO}_3$  (distorted tetrahedral), suggesting a distorted tetrahedral coordination in this particular 1 wt.% V/AC sample. The pre-edge peak height decreases with the increase in the vanadium loading. For the 4 wt.% V/AC sample, the pre-edge height is 0.43, which is close to that of  $\text{PbV}_2\text{O}_6$  (0.45) with octahedral coordination. With further increasing the V-content, the pre-edge peak height remains at around 0.42, implying the consistent chemical environment in an octahedral symmetry for all the rest high-loading V/AC samples.

The energy shift of the pre-edge peak from the main-edge is a measurement of vanadium oxidation state [41]. It is reported that the  $E_{\text{edge}} - E_{\text{pre-edge}}$  value is between 12.4 eV and 12.8 eV for the tetrahedral vanadium (5+), 11.5 eV for the octahedral vanadium (5+) as in  $\text{PbV}_2\text{O}_6$ , and 9.5 eV for the square pyramidal vanadium (5+) as in  $\text{V}_2\text{O}_5$  [41]. For the vanadium compound with lower oxidation state, this value dramatically decreases as follows: 8.2 eV for  $\text{VOSO}_4 \cdot 3\text{H}_2\text{O}$  and 5.8 eV for  $\text{V}_2\text{O}_3$ . For the 1 wt.% V/AC sample, the energy shift is 12.1 eV, implying a tetrahedral coordinated vanadium under 5+ oxidation state. The  $E_{\text{edge}} - E_{\text{pre-edge}}$  values of the V/AC samples with high V loadings (greater than 4 wt.%) vary between 11.5 eV and 11.9 eV, indicating the presence of octahedral vanadium (5+) species. This value is remarkably higher than that of  $\text{V}_2\text{O}_5$  with a square pyramidal coordination, which may rule out the existence of measurable aggregated  $\text{V}_2\text{O}_5$  (9.5 eV) on the carbon surface. These results are in accordance with XRD measurements.

Empirically, the strength of the pre-edge transition has been found to be related to the size of the “molecular cage” [41]. The pre-edge peak intensities of the V/AC samples are summarized in Table 1. The pre-edge peak intensity of the 1 wt.% V/AC sample resembles that of reference  $\text{NH}_4\text{VO}_3$  with a distorted tetrahedral coordination, which indicates the vanadium domains in this sample possess a similar cage size to that of  $\text{NH}_4\text{VO}_3$ . The pre-edge intensities of other V/AC samples with high V loadings (greater than 4 wt.%) are close to that of  $\text{PbV}_2\text{O}_6$  with an octahedral coordination.

Fourier transforms of the  $K^3$ -weighted vanadium K-edge EXAFS spectra (without phase shift correction) of the V/AC samples along with  $\text{V}_2\text{O}_5$  reference are shown in Fig. 4, and the corresponding curve-fitting results are listed in Table 2. The  $\text{V}_2\text{O}_5$  reference spectrum shows a weak peak at 1.1 Å and a strong peak at 1.5 Å assignable to V–O bonds in the first shell; features at approximately 2.8 and 3.3 Å are attributed to V–O–V through edge-shared and corner-shared  $\text{VO}_5$  square pyramids, respectively [42]. As shown in Table 2, the average coordination number (CN) for the first V–O shell of  $\text{V}_2\text{O}_5$  is close to 5, one V–O bond length is around 1.58 Å and three V–O bond lengths are between 1.83 and 1.95 Å. These curve-fitting results are in good agreement with the crystallographic data reported elsewhere [43], confirming the validity of spectrum analyses in this study. The 1 wt.% V/AC sample shows a sharp and intense peak of V–O at 1.2 Å. The curve-fitting data shows that vanadium in this sample is in a four-coordination state with the lengths of four V–O bands between 1.61 and 1.74 Å. As vanadium content increases to 4 wt.% and above, the EXAFS peak assigned to V–O bonds become appreciably broad and a shoulder peak at high  $R$  appears, suggesting a dramatic change of the local coordination of vanadium species. The curve-fitting analysis of the 4 wt.% V/AC sample shows that the coordination number for the first V–O shell is about 4.5, implying the coexistence of tetrahedral and octahedral vanadium (5+) species. With further increase in the vanadium loading to 10 wt.%

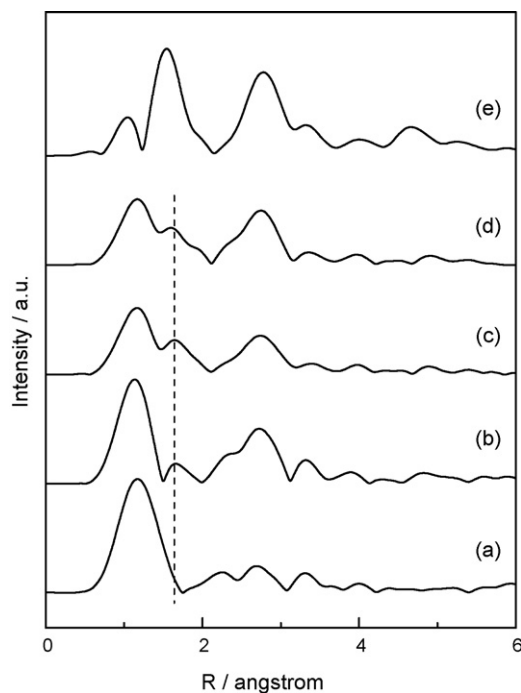


Fig. 4. Fourier transformed V K-edge EXAFS of the V/AC catalysts as well as  $\text{V}_2\text{O}_5$  (phase shift was not corrected): (a) 1 wt.% V/AC; (b) 4 wt.% V/AC; (c) 10 wt.% V/AC; (d) 20 wt.% V/AC; (e)  $\text{V}_2\text{O}_5$ .

and 20 wt.%, vanadium atoms change mainly into the octahedral coordination because the first shell V–O coordination number is close to 6.0 (see Table 2).

### 3.4. XPS results

The V 2p<sub>3/2</sub> photoelectron peaks of the V/AC catalysts are shown in Fig. 5. The binding energy of V 2p<sub>3/2</sub> is 517.5 eV for the V/AC samples with vanadium loadings below 2 wt.%, meaning the  $\text{V}^{5+}$  species predominate [44]. With increasing V loadings from 2 to 20 wt.%, a slight shift of binding energy from 517.5 to 517.2 eV occurs. This shift in binding energy with the increase in vanadium loading may be due to the presence of  $\text{V}^{4+}$  species as discussed later using ESR.

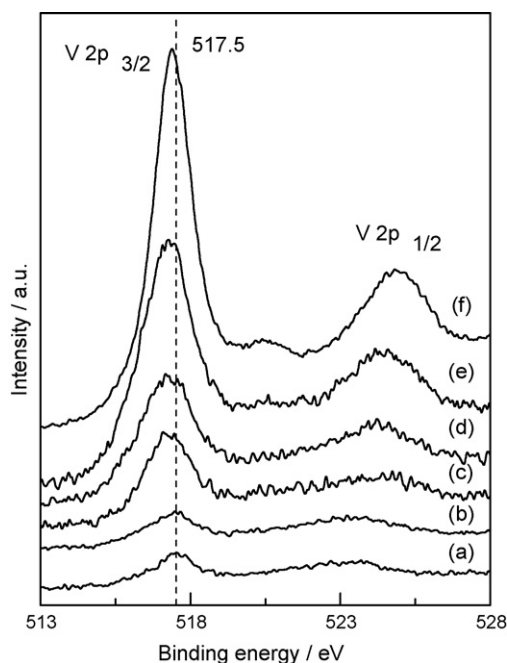
Fig. 6 shows the comparison of V:C atomic ratio determined by XPS to that of ICP results as a function of the vanadium load-

Table 2  
Results of V K-edge EXAFS curve-fitting analyses for the V–O shells of the V/AC catalysts<sup>a</sup>.

Samples	CN ( $\pm 10\%$ )	R (Å) ( $\pm 0.01$ )	$\sigma^2$ (Å <sup>2</sup> ) ( $\pm 10\%$ )	R-factor
$\text{V}_2\text{O}_5$	1.0	1.55	0.0013	0.088
	1.4	1.83	0.0005	
	2.5	1.95	0.0042	
1 wt.% V/AC	2.5	1.61	0.0031	0.071
	1.3	1.74	0.0008	
4 wt.% V/AC	2.1	1.60	0.0003	0.083
	1.5	1.73	–0.0025	
	0.9	1.87	–0.0026	
10 wt.% V/AC	1.1	1.57	–0.0007	0.097
	2.5	1.73	0.0020	
	2.3	1.89	0.0022	
20 wt.% V/AC	1.1	1.55	0.0005	0.088
	1.9	1.76	0.0028	
	3.0	1.89	0.0033	

<sup>a</sup> CN, R, and  $\sigma^2$  are coordination number, bond length and Debye–Waller factor, respectively; R-factor is the residual of fit.





**Fig. 5.** XPS spectra of the V 2p region for the V/AC catalysts along with  $V_2O_5$ : (a) 1 wt.% V/AC; (b) 2 wt.% V/AC; (c) 4 wt.% V/AC; (d) 10 wt.% V/AC; (e) 20 wt.% V/AC; (f)  $V_2O_5$ .

ing, yielding the information about the homogeneity of vanadium distribution [45]. For the V/AC samples with vanadium loadings below 4 wt.%, the V:C atomic ratios from XPS are close to that of ICP analysis, indicating that the vanadium species are homogeneously distributed [45], and preferentially located on the external surface of activated carbon. The vanadium species migrate into the internal channels of activated carbon for high V-content samples (>10 wt.%) because the V:C atomic ratios from XPS are remarkably lower than that determined by ICP analysis, thus leading to a noteworthy decrease in the BET surface area, as shown in Table 1.

### 3.5. ESR results

The ESR technique facilitates gaining more information about the oxidation state of vanadium species in these V/AC samples. The  $V^{4+}$  species, which exhibits hyperfine splitting due to interactions between electron spin ( $S = +1/2$ ) and nuclear spin ( $I = +7/2$ ),

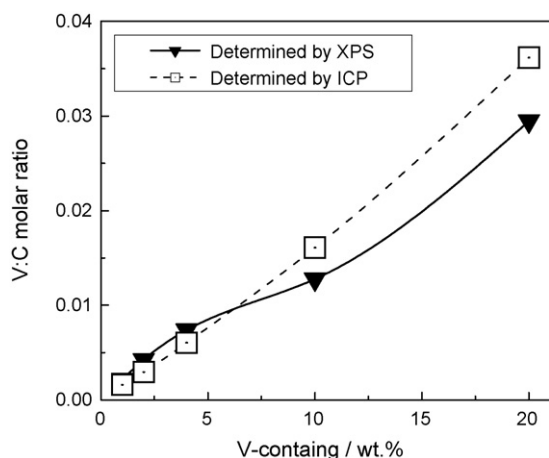


**Fig. 6.** V:C atomic ratios as a function of the vanadium loading in the V/AC catalysts.

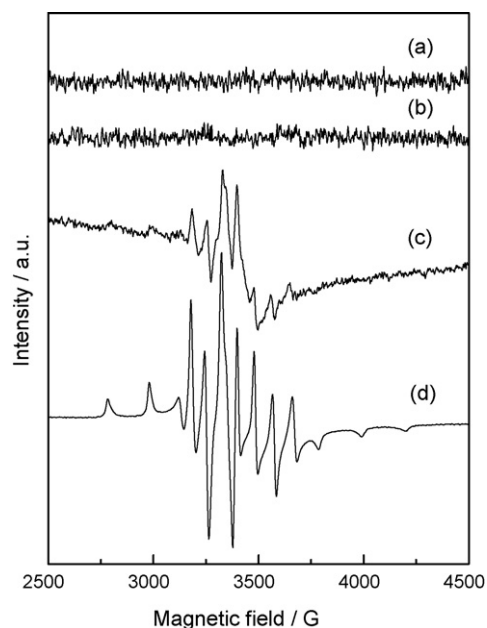


**Fig. 7.** ESR spectra of the V/AC catalysts: (a) 1 wt.% V/AC, (b) 2 wt.% V/AC, (c) 4 wt.% V/AC, and (d) 20 wt.% V/AC.

is a particularly useful probe to characterize the nature of support, the location and the symmetry of the site since its EPR spectrum is readily observable over a large temperature range [46]. The ESR spectra of the V/AC samples with different vanadium loadings measured at 77 K are depicted in Fig. 7. A well-resolved ESR spectra with  $g_{\parallel}$  and  $g_{\perp}$  lines of hyperfine structure can be observed in the sample with vanadium loading of 20 wt.%, indicating the presence of  $V^{4+}$  centers in a distorted tetrahedral symmetry [46]. The intensity of ESR signals decreases gradually as the vanadium loading decreases from 20 to 4 wt.%. This may be due to the decrease in the  $V^{4+}$  content at lower vanadium loadings. The absence of any ESR signal for the V/AC samples with vanadium content lower than 2 wt.% suggests that all vanadium species in these samples are presented as  $V^{5+}$ .

### 3.6. Catalytic results

The V/AC samples with different vanadium loadings have been examined for the aerobic oxidation of benzyl alcohol with molecular  $O_2$ . As shown in Table 3, the V/AC catalysts can effectively catalyze the conversion of benzyl alcohol under mild conditions, forming benzaldehyde as the main product along with trace amount of benzoic acid. Reactions performed under a nitrogen atmosphere do not proceed significantly beyond the stoichiometric amount of catalyst. With increasing vanadium loading from 1 to 4 wt.%, benzyl alcohol conversion substantially increases, and it reaches a maximum (85.4%) at the vanadium content of 4 wt.%. Further increasing V-content, however, lowers the benzyl alcohol conversion. As evidenced by XRD, Raman, and XPS, the vanadium species with vanadium loadings lower than 4 wt.% are highly dispersed on the external surface of activated carbon, whereas high vanadium contents (>10 wt.%) result in microcrystalline phase vanadium oxides located inside the internal channels, resulting in a remarkably poor catalytic activity. Therefore, it is likely that a higher dispersion of vanadium species results in higher catalytic activity. It is noted that the V/AC catalyst with the vanadium content of 1 wt.% shows the highest TOF of  $42.3 \text{ h}^{-1}$ . A noticeable decrease in TOF is observed with the increase in vanadium loading, especially when the vanadium content is higher than 4 wt.%. Based on XANES, EXAFS, XPS, and ESR characterizations, the vanadium ( $5+$ )

**Table 3**  
Effect of V-content on the catalytic properties of the V/AC catalysts in the oxidation of benzyl alcohol with O<sub>2</sub><sup>a</sup>.

Catalyst	S <sub>BET</sub> (m <sup>2</sup> /g)	Benzyl alcohol conv. (%)	Benzaldehyde select. (%)	TOF <sup>b</sup> (h <sup>-1</sup> )
AC	856	0.6	>99	–
1 wt.% V/AC	854	46.5	>99	42.3
2 wt.% V/AC	823	66.9	>99	30.4
4 wt.% V/AC	770	85.4	>99	19.4
4 wt.% V/AC <sup>c</sup>	770	13.1	>99	3.0
7 wt.% V/AC	704	75.5	>99	9.8
10 wt.% V/AC	662	75.6	>99	6.9
20 wt.% V/AC	432	73.5	>99	3.3

<sup>a</sup> Reaction conditions: the amount of catalyst, 0.2 g; benzyl alcohol, 2 mmol; O<sub>2</sub> flow rate, 10 ml min<sup>-1</sup>; reaction temperature, 373 K; reaction time, 2 h.<sup>b</sup> TOF was evaluated from the moles of the substrate converted per mol V<sub>2</sub>O<sub>5</sub> in catalyst per hour.<sup>c</sup> Blank experiment under inert N<sub>2</sub>.**Table 4**  
Oxidation of benzyl alcohol with O<sub>2</sub> catalyzed by the vanadium-containing catalysts<sup>a</sup>.

Catalyst	Benzyl alcohol conv. (%)	Benzaldehyde select. (%)	TOF <sup>b</sup> (h <sup>-1</sup> )
4 wt.% V/AC	85.4	>99	19.4
4 wt.% V/SiO <sub>2</sub>	4.2	>99	0.9
4 wt.% V/SBA-15	4.8	>99	1.1
4 wt.% V/Al <sub>2</sub> O <sub>3</sub>	7.7	>99	1.7
4 wt.% V/ZrO <sub>2</sub>	4.9	94.5	1.1
4 wt.% V/TiO <sub>2</sub>	51.7	97.4	11.7

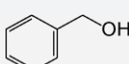
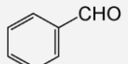
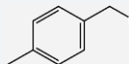
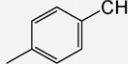
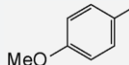
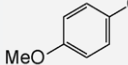
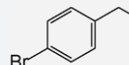
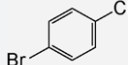
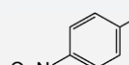
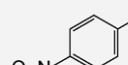
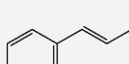
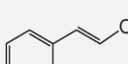
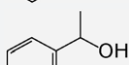
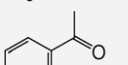
<sup>a</sup> Reaction conditions: the amount of catalyst, 0.2 g; benzyl alcohol, 2 mmol; O<sub>2</sub> flow rate, 10 ml min<sup>-1</sup>; reaction temperature, 373 K; reaction time, 2 h.<sup>b</sup> TOF was evaluated from the moles of the substrate converted per mol V<sub>2</sub>O<sub>5</sub> in catalyst per hour.

species on activated carbon surface show a similar local coordination structure to that of NH<sub>4</sub>VO<sub>3</sub> with a distorted tetrahedral symmetry at a low vanadium loading of 1 wt.%, whereas octahedral coordination vanadium (5+) species is dominant at high vanadium loadings (>4 wt.%). Hence, the vanadium (5+) species with a distorted tetrahedral coordination are more active than octahedral ones in the aerobic oxidation of alcohols. Yang and Lunsford [47]

have proposed a mechanism for the oxidation of methanol over the vanadium oxides surface. The main step involved in the catalytic cycle is the abstraction of methyl hydrogen by catalytic surface oxygen, followed by rapid intramolecular rearrangement and desorption of formaldehyde and other products. This step is widely accepted in the literature [48–51]. Reddy et al. [48] have also proved that coordinatively unsaturated V-oxide sites are the locations for the initial dissociative adsorption of methanol. The alcohol oxidation activity trends observed in this study clearly indicate that coordinatively unsaturated V-oxide sites (tetrahedral vanadium) are the locations for the initial dissociative adsorption of alcohols following the above mentioned mechanism [47]. Therefore, it is reasonable to suggest that highly dispersed vanadium (5+) species with a distorted tetrahedral coordination on carbon surface account for the superior catalytic performance of the V/AC catalysts.

In this study, various catalyst supports, e.g., Al<sub>2</sub>O<sub>3</sub>, ZrO<sub>2</sub>, TiO<sub>2</sub>, SiO<sub>2</sub>, and SBA-15, have also been used to prepare vanadium-loaded catalysts by the same precipitation method. Despite similar characteristics of surface vanadium species on different supports, their catalytic performances are substantially different as shown in Table 4. Among the supports studied, active carbon exhibits

**Table 5**  
Catalytic properties of 4 wt.% V/AC for the oxidation of various alcohols with O<sub>2</sub><sup>a</sup>.

Entry	Substrate	Product	Time (h)	Conversion (%)	Selectivity (%)	TOF <sup>b</sup> (h <sup>-1</sup> )
1			3	>99	>99	15.1
2			3	99	>99	15.0
3			2.5	>99	>99	18.1
4			2.5	>99	>99	18.1
5			2	>99	>99	22.7
6			3	>99	>99	15.1
7			8	97	>99	5.5

<sup>a</sup> Reaction conditions: the amount of catalyst, 0.2 g; reaction temperature, 373 K; substrate, 2 mmol; O<sub>2</sub> flow rate, 10 ml min<sup>-1</sup>.<sup>b</sup> TOF was evaluated from the moles of the substrate converted per mol V<sub>2</sub>O<sub>5</sub> in catalyst per hour.

the highest benzyl alcohol conversion and benzaldehyde selectivity. In the aerobic oxidation of alcohols by vanadium-containing catalysts, the reaction is considered to proceed by the transfer of electrons and a proton from substrate to the catalyst, yielding product and a proton and reduced catalyst. The reduced catalyst is reoxidized by dioxygen, yielding water and completing the catalytic cycle [52]. The high catalytic activity on the active carbon is believed to be due to the higher concentration of substrates and oxygen by the adsorption in the vicinity of the active site. In addition, the electrons can easily transfer from the substrates to the catalyst on the active charcoal, since the active carbon can serve as a good mediator of the electron transfer [53].

To assess the scope of this particular V/AC catalyst, the oxidation of a variety of aromatic alcohols has been studied on 4 wt.% V/AC at 373 K. As shown in Table 5, aromatic alcohols are oxidized giving the corresponding aldehydes with high conversion (entries 1–5). Substituted aromatic alcohol compounds containing electron-donating or -withdrawing groups (such as,  $-\text{CH}_3$ ,  $-\text{OCH}_3$ ,  $-\text{Br}$  or  $-\text{NO}_2$ ) are more readily oxidized than that of un-substituted aromatic alcohols. Note that 4 wt.% V/AC also displays a high catalytic activity for oxidizing allylic alcohols, e.g., cinnamyl alcohol is selectively oxidized to cinnamyl aldehyde (with 99% conversion in 3 h; entry 6). Although secondary alcohols, e.g., 1-phenylethanol, are less reactive in comparison with benzylic alcohols or allylic alcohols, they can also be oxidized to the respective ketones with high yields at a longer reaction time (entry 7). Neumann and Levin [52] have reported that the oxidation of alcohols on vanadium-containing catalysts is considered to proceed by transfer of electrons and a proton from substrate to the catalyst, yielding product and a proton and reduced catalyst. The higher catalytic activity of the substrates having both electron-donating and electron-withdrawing groups in the aromatic ring, such as 4-methyl-, 4-methoxy-, 4-nitro-, and 4-bromobenzyl alcohols is believed to be due to that the electron can be more easily transferred from the substrate to the catalyst.  $\text{V}-\text{O}-\text{CH}_3$  has been reported to form upon the methanol oxidation on vanadium oxide catalysts [54]. Wang and Madix [49] have suggested that the transition state for  $\text{V}-\text{O}-\text{CH}_3$  involves a five-member ring which is a common intermediate structure proposed for organic reactions. 1-Phenylethanol, because of space effects, may be not easy to form a similar five-member ring transition state, thus resulting in a lower conversion.

#### 4. Conclusion

The activated carbon-supported vanadium oxide catalysts were synthesized by a conventional wet-impregnation method. Various characterizations revealed that this preparation mainly resulted in highly dispersed vanadium (5+) species homogeneously distributed on the activated carbon surface below 10 wt.% vanadium content. Less vanadium oxides on the carbon external surface showed a similar coordination structure compared to  $\text{NH}_4\text{VO}_3$  with a distorted tetrahedral symmetry, whereas the microcrystalline phase vanadium (5+) oxides located inside the channels appeared at higher vanadium loadings (above 10 wt.%), the vanadium species stayed in the octahedral coordination local environment. Moreover, the  $\text{V}^{5+}$  species predominated in all V/AC samples, and  $\text{V}^{4+}$  centers in a distorted tetrahedral symmetry could be observed at higher vanadium loadings (greater than 4 wt.%). Highly dispersed vanadium (5+) species with a distorted tetrahedral coordination on carbon external surface were suggested to be the active sites in the aerobic oxidation of aromatic alcohols with molecular  $\text{O}_2$ .

#### Acknowledgments

This work was mainly supported by AcRF grant tier 2 ARC 13/07. Work partially performed at SSLS under NUS Core Support C-380-003-003-001, A\*STAR/MOE RP 3979908M and A\*STAR 12 105 0038 grants.

#### References

- [1] F. Roozeboom, P.D. Cordingley, P.J. Gellings, *J. Catal.* 68 (1981) 464–472.
- [2] R. Neumann, M. Levin, *J. Org. Chem.* 56 (1991) 5707–5710.
- [3] S. Velusamy, T. Punniyamurthy, *Org. Lett.* 6 (2004) 217–219.
- [4] L. Rout, P. Nath, T. Punniyamurthy, *Adv. Synth. Catal.* 349 (2007) 846–848.
- [5] J. Dobler, M. Pritzsche, J. Sauer, *J. Am. Chem. Soc.* 127 (2005) 10861–10868.
- [6] R.Z. Khaliullin, A.T. Bell, *J. Phys. Chem. B* 106 (2002) 7832–7838.
- [7] Y.H. Yang, G.A. Du, S.Y. Lim, G.L. Haller, *J. Catal.* 234 (2005) 318–327.
- [8] G.A. Du, Y.H. Yang, W. Qiu, S. Lim, L. Pfeferle, G.L. Haller, *Appl. Catal. A: Gen.* 313 (2006) 1–13.
- [9] G.A. Du, S.Y. Lim, Y.H. Yang, C. Wang, L. Pfeferle, G.L. Haller, *Appl. Catal. A: Gen.* 302 (2006) 46–61.
- [10] Q.H. Tang, C. Wang, S.Q. Hu, H. Sun, Y. Chen, G.L. Haller, Y.H. Yang, *Catal. Lett.* 117 (2007) 25–33.
- [11] T. Blasco, J.M.L. Nieto, *Appl. Catal. A: Gen.* 157 (1997) 117–142.
- [12] N.R. Shiju, M. Anilkumar, S.P. Mirajkar, C.S. Gopinath, B.S. Rao, C.V. Satyanarayana, *J. Catal.* 230 (2005) 484–492.
- [13] I.E. Wachs, R.Y. Saleh, S.S. Chan, C.C. Chersich, *Appl. Catal.* 15 (1985) 339–352.
- [14] J.N. Armor, *Appl. Catal. B: Environ.* 1 (1992) 221–256.
- [15] J.P. Dunn, P.R. Koppula, H.G. Stenger, I.E. Wachs, *Appl. Catal. B: Environ.* 19 (1998) 103–117.
- [16] B.N. Reddy, B.M. Reddy, M. Subrahmanyam, *J. Chem. Soc. Faraday Trans.* 87 (1991) 1649–1655.
- [17] M.D. Amiridis, R.V. Duevel, I.E. Wachs, *Appl. Catal. B: Environ.* 23 (1999) 111–122.
- [18] B.C. Huang, R. Huang, D.J. Jin, D.Q. Ye, *Catal. Today* 126 (2007) 279–283.
- [19] Z.P. Zhu, Z.Y. Liu, H.X. Niu, S.J. Liu, T.D. Hu, T. Liu, Y.N. Xie, *J. Catal.* 197 (2001) 6–16.
- [20] E. Garcia-Bordeje, L. Calvillo, M.J. Lazaro, R. Moliner, *Appl. Catal. B: Environ.* 50 (2004) 235–242.
- [21] G.C. Bond, S.F. Tahir, *Appl. Catal.* 71 (1991) 1–31.
- [22] N.K. Nag, K.V.R. Chary, B.M. Reddy, B.R. Rao, V.S. Subrahmanyam, *Appl. Catal.* 9 (1984) 225–233.
- [23] B.M. Reddy, P.M. Sreekanth, E.P. Reddy, Y. Yamada, Q.A. Xu, H. Sakurai, T. Kobayashi, *J. Phys. Chem. B* 106 (2002), pp. 5695–5670.
- [24] L.R. Radovic, F. Rodriguez-Reinoso, in: P.A. Thrower (Ed.), *Chemistry and Physics of Carbon*, 25, Dekker, New York, 1997, p. 243.
- [25] J. Ogonowski, E. Skrzynska, *Catal. Lett.* 124 (2008) 52–58.
- [26] S.V. Vassilev, C. Braekman-Danheux, R. Moliner, I. Suelves, M.J. Lazaro, T. Thiemann, *Fuel* 81 (2002) 1281–1296.
- [27] T. Valdes-Solis, G. Marban, A.B. Fuertes, *Appl. Catal. B: Environ.* 46 (2003) 261–271.
- [28] M.E. Galvez, M.J. Lazaro, R. Moliner, *Catal. Today* 102 (2005) 142–147.
- [29] Y.X. Guo, Z.Y. Liu, Q.Y. Liu, Z.G. Huang, *Catal. Today* 131 (2008) 322–329.
- [30] E. Garcia-Bordeje, M.J. Lazaro, R. Moliner, J.F. Galindo, J. Sotres, A.M. Baro, *J. Catal.* 223 (2004) 395–403.
- [31] S. Pinto, L. D'Ornelas, P. Betancourt, *Appl. Surf. Sci.* 254 (2008) 5390–5393.
- [32] H.O. Moser, B.D.F. Casse, E.P. Chew, M. Cholewa, C.Z. Diao, S.X.D. Ding, J.R. Kong, Z.W. Li, M. Hua, M.L. Ng, B.T. Saw, S. Bin Mahmood, S.V. Vidyaraj, O. Wilhelmi, J. Wong, P. Yang, X.J. Yu, X.Y. Gao, A.T.S. Wee, W.S. Sim, D. Lu, R.B. Faltermeier, *Nucl. Instr. Method B* 238 (2005) 83–86.
- [33] S.I. Zabinsky, J.J. Rehr, A. Ankudinov, R.C. Albers, M.J. Eller, *Phys. Rev. B* 52 (1995) 2995–3009.
- [34] Q.H. Tang, T. Liu, Y.H. Yang, *Catal. Commun.* 9 (2008) 2570–2573.
- [35] Q. Tang, et al., *J. Mol. Catal. A: Chem.* (2008), doi:10.1016/j.molcata.2008.11.003.
- [36] C.B. Rodella, R.W.A. Franco, C.J. Magon, J.P. Donoso, L.A.O. Nunes, M.J. Saeki, M.A. Aegerter, V. Sargentelli, A.O. Florentino, *J. Sol-Gel Sci. Technol.* 25 (2002) 83–88.
- [37] G.A. Du, S.Y. Lim, M. Pinault, C. Wang, F. Fang, L. Pfeferle, C.L. Haller, *J. Catal.* 253 (2008) 74–90.
- [38] L. Abello, E. Husson, Y. Repelin, G. Lucazeau, *Spectrochim. Acta Part A* 39 (1983) 641–651.
- [39] N. Das, H. Eckert, H.C. Hu, I.E. Wachs, J.F. Walzer, F.J. Feher, *J. Phys. Chem.* 97 (1993) 8240–8243.
- [40] G.T. Went, S.T. Oyama, A.T. Bell, *J. Phys. Chem.* 94 (1990) 4240–4246.
- [41] J. Wong, F.W. Lytle, R.P. Messmer, D.H. Maylotte, *Phys. Rev. B* 30 (1984) 5596–5610.
- [42] T. Tanaka, H. Yamashita, R. Tsuchitani, T. Funabiki, S. Yoshida, *J. Chem. Soc., Faraday Trans. 1* 84 (1988) 2987–2999.
- [43] Q.H. Zhang, W. Yang, X.X. Wang, Y. Wang, T. Shishito, K. Takehira, *Micropor. Mesopor. Mater.* 77 (2005) 223–234.
- [44] V.I. Bukhtiyarov, *Catal. Today* 56 (2000) 403–414.
- [45] P. Oliveira, M.L. Rojas-Cervantes, A.M. Ramoa, I.M. Fonseca, A.M. Botelho do Rego, *J. Vital. Catal. Today* 118 (2006) 307–314.

- [46] K.V.R. Chary, G. Kishan, C.P. Kumar, G.V. Sagar, *Appl. Catal. A: Gen.* 246 (2003) 335–350.
- [47] T.J. Yang, J.H. Lunsford, *J. Catal.* 103 (1987) 55–64.
- [48] E.P. Reddy, R.S. Varma, *J. Catal.* 221 (2004) 93–101.
- [49] Q.G. Wang, R.J. Madix, *Surf. Sci.* 496 (2002) 51–63.
- [50] J.L. Bronkema, A.T. Bell, *J. Phys. Chem. C* 111 (2007) 420–430.
- [51] Y. Romanyshyn, S. Guimond, H. Kuhlenbeck, S. Kaya, R.P. Blum, H. Niehus, S. Shaikhutdinov, V. Simic-Milosevic, N. Nilius, H.I. Freund, M.V. Ganduglia-Pirovano, R. Fortrie, J. Dobler, J. Sauer, *Top. Catal.* 50 (2008) 106–115.
- [52] R. Neumann, M. Levin, *J. Am. Chem. Soc.* 114 (1992) 7278–7286.
- [53] R.A. Sheldon, J.K. Kochi, *Metal Catalyzed Oxidations of Organic Compounds*, Academic Press, New York, 1981, p. 271.
- [54] G. Busca, A.S. Elmi, P. Forzatti, *J. Phys. Chem.* 91 (1987) 5263–5269.